Snap-through of a bistable beam using piezoelectric actuators: modeling and optimization

A. Amor, Amâncio Fernandes, J. Pouget

Snap-through of a bistable beam using piezoelectric actuators : modeling and optimization

A. Amor[a], A. Fernandes[a,*], and J. Pouget[a]

[a]Sorbonne Université, CNRS, Institut Jean le Rond d'Alembert, UMR 7190, F-75005 Paris, France;
[*]Corresponding author, amancio.fernandes@sorbonne-universite.fr

Abstract

In the study, we report the snap-through effect of a bistable beam by means of piezoelectric actuators. We first consider a bistable mechanism consisting of a buckled elastic thin beam. The latter is symmetrically equipped with two piezoelectric layers. The electric potential applied on the faces of the piezoelectric actuators is such as a moment at each end of the active layers is produced. The modeling of the elastic beam is based on the elastica theory. The main goal of the study is the investigation of the bistable response according to the applied electric voltage and the configurational parameters. A numerical study is proposed based on the equation of the beam model sandwiched by two piezoelectric layers and a numerical validation of the model approach is performed using the finite element method. An optimization study is reported for the placement of the piezoelectric actuators as well as their dimensions (length and thickness). We look for the position of the piezoelectric actuators that minimizes the applied voltage to trigger the snap-through and maximize the beam deflection. The work is extended to the bistable actuation using two pairs of piezoelectric elements.

Keywords : Bistable beam; buckling; snap-through; piezoelectric actuation; optimization.

1 Introduction

The design of bistable mechanisms has been developed due to the growing interest in advanced technology such as robotics, medical engineering, and the technology of micro-electro-mechanical systems (MEMS) [Cao et al., 2021, Charlot et al., 2008, Pane and Asano, 2008]. The bistable mechanisms are mechanical components involved in a large variety of cutting-edge engineering applications. Thanks to the new technology of layer deposit, the design MEMS is quite realizable such as micro-robotics, medical endoscopy, non-volatil memories, micro-switches, tactile displays for visually impaired people [Chouvardas et al., 2008, Feng and Hou, 2018, Vitushinsky et al., 2009]. The snap-through property of the bistable structures can be exploited for shape control applications [Emam and Inman, 2015, Fernandes et al., 2010, Schoeftner et al., 2015, Zhang et al., 2019]. Moreover, in the case of the bistable structures equipped with piezoelectric sensors, the bistable can be used for energy harvesting converting the bistable dynamics into usable electric energy [Anton and Sodano, 2007, Cook-Chennault et al., 2008, Cottone et al., 2009]. This kind of device is convenient as a power source for wireless sensor networks.

The buckled configuration of an elastic beam is obtained by imposing a small end-shortening caused by a compressive force applied in the direction of the beam axis at one of the ends of the beam. As soon as the buckling force exceeds a critical value, the straight configuration of the beam is no

longer stable, and the beam undergoes a deflection (in the transverse direction) [Bažant et al., 1991, Bigoni, 2012, Dym, 2002, Thompson and Hunt, 1973, Timoshenko and Gere, 1963]. We say that we have a bifurcation phenomenon, resulting in the buckling of the beam [Timoshenko and Gere, 1963]. The latter can deflect either upwards or downwards. These new configurations of the beam are stable states. Nevertheless, the most interesting property of such a buckled beam is to be able to switch from one stable state to another regardless of how the transition is completed (switching process is obtained). The simplest way of switching the bistable beam is to apply a punctual force at a curvilinear point of the deformed beam in the transverse direction [Camescasse et al., 2013]. The applied transverse force triggers the beam snap-through from one stable buckled beam (upwards or downwards) to the other stable state and *vice versa*. Moreover, the force can be easily replaced by a punctual moment applied at a curvilinear point of the beam [Cazottes et al., 2009].

Active material such as piezoelectric ceramics, shape memory alloys, magnetostrictive materials or electro-active polymers open new opportunities for the bistable actuation. Among the smart materials, piezoelectric ceramics are the most popular, they can be used as sensors and/or actuators. However, they suffer drawbacks, especially, since materials have limited actuating strokes (small displacement and strain) in their first-order linear behavior, namely, for reasonable applied electric potential differences. Furthermore, piezoelectric actuators incorporated in a prestressed structures, such as a buckled beam, is a mean to release the energy stored in prestressing process to amplify the action of the piezoelectric material. For bistable beams, the role of the actuator allows one to trigger the snap-through from one stable state to the other with the use of rather small amount of energy. This concept has been used for designing MEMS switches, relays, etc. [Chen et al., 2011, Fu et al., 2007, Roodenburg et al., 2009]. The actuation of a bistable beam using piezoelectric actuators has been proposed by [Aimmanee and Tichakorn, 2018, Maurini et al., 2007]. Other actuation devices proposed in the literature exploit different kinds of actuating forces such as electrostatic forces which are effective only at the microscopic scale [Chen and Meguid, 2015, Krylov et al., 2011, Park and Hah, 2008, Younis et al., 2010] with extension to microscopic arch-shaped beams [Krylov and Dick, 2010, Ouakad, 2014, Ramini et al., 2016, Wu et al., 2014]. Micro-beams actuated by electro-thermo-mechanical effect or by shape memory alloys heated by laser are presented by Barth and Zaidi [Barth et al., 2010, Zaidi et al., 2012]. The contactless actuation of a bistable beam utilizing the electromagnetic Laplace force has been reported by [Amor et al., 2020, 2022]. In the same spirit, [Abbasi et al., 2023] investigate the snap-through of a magneto-active beam subject to the combined mechanical and magnetic actuation.

The present work aims to investigate the switching response of the bistable beam actuated by piezoelectric layers. More precisely, we characterize the beam deflection as a function of the electric potential difference applied to piezoelectric actuators according to the actuator location and their geometrical parameters. Our modeling approach is based on elastica theory for a one-dimensional elastic beams [Chen and Tsao, 2013, 2014, Goss, 2009, Magnusson et al., 2001, Patricio et al., 1998], which allows us to account for large rotations of the beam cross-section. A correct switching approach of the bistable beam must account for the effect of the beam extensibility [Camescasse et al., 2013]. Particular attention is paid to the modeling of the region of the beam sandwiched by the piezoelectric layers accounting for the strain-stress transverse effect. The material is considered in its linear regime and the piezoelectric effect is modeled by flexural induced strain, which is evaluated by means of an equivalent single-layer beam theory based on Bernoulli-Euler assumption. We show that the action of the piezoelectric layers placed symmetrically on the upper and lower faces of the central layer is modeled by moments applied at the ends of the piezoelectric

actuators. In [Maurini et al., 2007], the authors propose the snap-through of a bistable beam using the piezoelectric actuators and the stability control of the switching process. Using the same kind of idea, the stabilization of higher-order buckling modes using piezoelectric patches has been reported by Xiu *et al.* [Xiu and Davis, 2021]. One of the most attractive developments of the bistable structures equipped with piezoelectric actuators is their ability to be miniaturized from a millimeter scale to dimensions of the order of a few microns. Extension to shallow elastic arches has been considered for the shape and the vibration control [Younis et al., 2010]. Similarly, we can point to the snap-through of shallow shells using piezoelectric Macro Fiber Composite actuators was investigated numerically and experimentally by [Anilkumar et al., 2021, Bowen et al., 2011, Schultz and Hyer, 2003].

The paper is organized as follows. The next Section provides all the ingredients that will be useful for the forthcoming developments of the model, especially, the kinematic and the electrical parameters. Section 3 is devoted to the variational formulation of the bistable beam symmetrically equipped with a pair of piezoelectric elements. Section 4 reports the numerical method for solving the equilibrium equations. The optimization of the actuator location and its dimensions are also described in Section 4. The extension to the bistable actuation by means of two pairs of piezoelectric layers and the bistable response, namely, the beam deflection as function of the applied difference of the electric potential is proposed subsequently. The conclusions are given in Section 5.

2 Description of the structure

2.1 Kinematic consideration

The bistable mechanism proposed in the present study consists of an isotropic and homogeneous elastic beam clamped at its ends. The beam length at rest is L_0, the width is b and the thickness is h_e. The beam is equipped with two identical piezoelectric layers symmetrically bonded on both sides of the elastic beam. The geometrical parameters of the piezoelectric layers are given in Figure 1.a with a length L_p, thickness h_p, and their widths are identical to that of the elastic layer. For both piezoelectric layers, their upper and lower faces are covered by very thin metal electrodes. The latter are connected to a voltage power supply so that the electric potential differences are the same for both piezoelectric layers made of an isotropic transverse material polarized along the thickness but in opposite direction.
The beam undergoes an end-shortening ΔL due to an applied compressive force that reduces the distance between the clamps.

The slender structure is modeled as an extensible and flexible beam undergoing plan deformation. A fixed Cartesian reference frame $\mathcal{R}_0 : \{A; \vec{e}_1, \vec{e}_2, \vec{e}_3\}$ is attached to the straight reference configuration, with the unit vector $\vec{e}_1$ in the direction of the beam axis. In its reference frame the beam is at rest, and a material point G_0 is given by the vector $\overrightarrow{AG}_0 = \vec{q}_0(s) = s\ \vec{e}_1$ with $s \in [0, L_0]$, where s is the abscissa along the beam axis. Once the beam buckled, the point G_0 is transformed into G in the current reference frame. The point G is then given by

$$\overrightarrow{AG}(s) = \vec{q}(s) = x(s)\,\vec{e}_1 + y(s)\,\vec{e}_2\,, \qquad s \in [0, L]\,, \tag{1}$$

The buckled beam and the different geometrical elements and applied loads are shown in Figure 1.b.

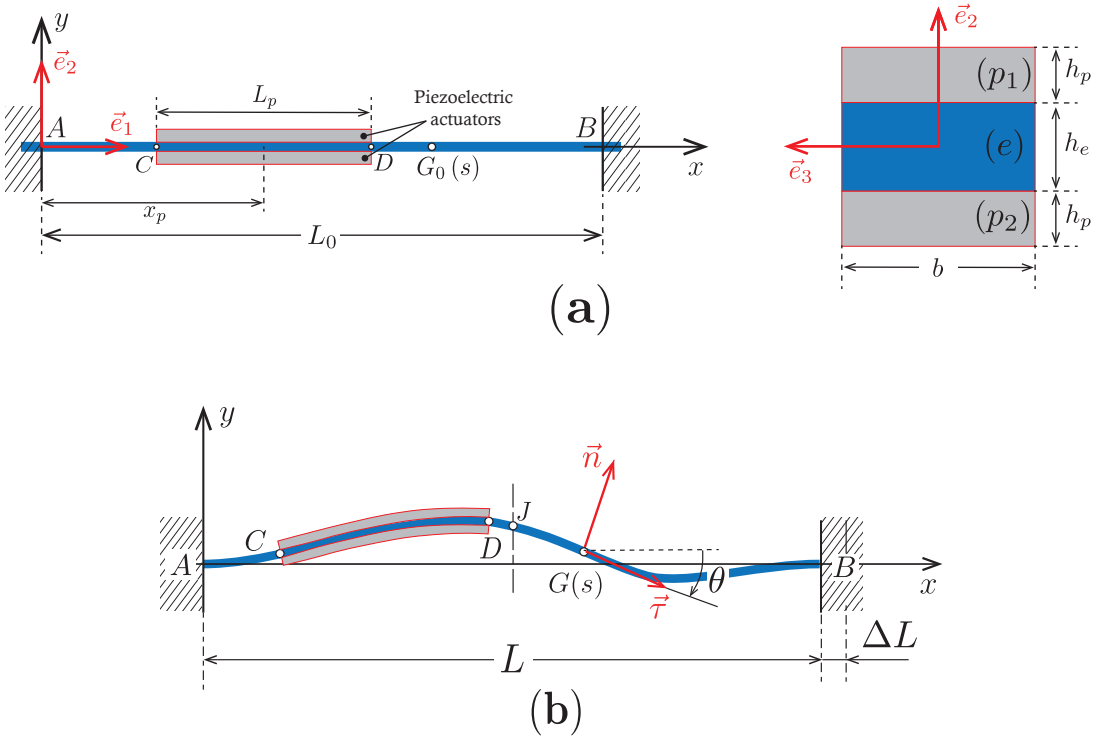

Figure 1: clamped-clamped elastic beam sandwiched by 2 piezoelectric layers: (a) the non loaded beam, (b) beam in its buckled configuration equipped with a pair of piezoelectric layers exhibiting the geometrical parameters.

From the mechanical point of view, the extensional strain ε and the beam curvature κ are chosen as the two strain measures. They are given by

$$\varepsilon(s) = \frac{d\bar{s} - ds}{ds} = \Lambda - 1\,, \tag{2}$$

$$\kappa(s) = \frac{d\vec{\tau}}{d\bar{s}} \cdot \vec{n}\,, \tag{3}$$

where $\Lambda = \frac{d\bar{s}}{ds}$ is the ratio of the length of differential line element of the beam in the current configuration to that of the undeformed configuration, $\bar{s}$ being the curvilinear coordinate measured along the deformed beam.
We denote by

$$\vec{\tau}(s) = \cos\theta(s)\vec{e}_1 + \sin\theta(s)\vec{e}_2\,, \tag{4a}$$

$$\vec{n}(s) = -\sin\theta(s)\vec{e}_1 + \cos\theta(s)\vec{e}_2\,, \tag{4b}$$

the tangent and normal vectors in the current configuration at the point of curvilinear abscissa s in the reference configuration, and θ is the angle formed by the tangent with $\vec{e}_1$.

2.2 Electric consideration

The piezoelectric actuators are placed symmetrically on the opposite sides of the elastic central layer. The latter is partly covered by piezoelectric layers on the section $[C, D]$ (see Figure 1.a). The piezoelectric layers are recovered by very thin metallic electrodes. The electric connections are such that the lower face of the upper piezoelectric layer and the higher face of the lower actuator

are at the potential zero. The higher face of the top layer and that of lower face are at the electric potential V. In this configuration, the metallic electrodes are equipotential surfaces. The electric fields are oriented in the thickness direction of both piezoelectric layers, and they are given by

$$\vec{E}_{p_1}(y) = E_{p_1}(y)\,\vec{e}_2\ , \tag{5a}$$

$$\vec{E}_{p_2}(y) = E_{p_2}(y)\,\vec{e}_2\ . \tag{5b}$$

The subscript p_1 refers as to the top piezoelectric layer while the subscript p_2 denotes the bottom piezoelectric layer. The electric fields derive from electric potentials as a function of the thickness coordinate such as

$$\vec{E}_{p_1}(y) = -\frac{d\phi_{p_1}}{dy}\,\vec{e}_2\,, \qquad \vec{E}_{p_2}(y) = -\frac{d\phi_{p_2}}{dy}\,\vec{e}_2\,, \tag{6}$$

where ϕ_{p_1} and ϕ_{p_2} are electric potential within the upper and lower layers, respectively. The variations of the electric potentials as a function of the thickness coordinate are given in Appendix A. Moreover, the electric potentials satisfy the boundary conditions on the piezoelectric layer electrodes, especially (see Figure 1.a for the geometrical parameters)

$$\text{layer } (p_1) \qquad \phi_{p_1}(\tfrac{h_e}{2}) = 0\,, \qquad \phi_{p_1}(\tfrac{h_t}{2}) = +V\,, \tag{7a}$$

$$\text{layer } (p_2) \qquad \phi_{p_2}(-\tfrac{h_e}{2}) = 0\,, \qquad \phi_{p_2}(-\tfrac{h_t}{2}) = +V\,, \tag{7b}$$

where $h_t = h_e + 2h_p$ is the total thickness of the sandwich beam section.

2.3 Variational formulation

The approach is based on the principle of the virtual work. The latter is stated as follows

$$\delta\mathcal{W}_i = 0\,, \tag{8}$$

where $\delta\mathcal{W}_i$ is the virtual work of the internal actions including mechanical and electrical loads. The composite beam is subject to no load except the buckling force to maintain the end-shortening at a given value.
The virtual work of the internal actions is deduced from the reduction of the 3D model of the composite beam to the 1D model of beam.

Moreover, the beam is divided into three sections, namely, $\mathcal{A}_1 = [0, s_C[$ the left elastic layer, $\mathcal{A}_2 =]s_C, s_D[$,the piezoelectric sandwich section and $\mathcal{A}_3 =]s_D, L]$ the right elastic layer.
On using the above notation, the virtual work takes on the form (for further details refer to [Amor et al., 2020, Camescasse et al., 2013]).

$$\delta\mathcal{W}_i = -\sum_{j=1}^{3}\int_{\mathcal{A}_j}\left\{\vec{R}^{(j)}(s)\cdot\delta\vec{q'}(s) + \vec{M}^{(j)}(s)\cdot\delta\vec{p'}(s) - \left(\vec{q'}(s)\times\vec{R}^{(j)}(s)\right)\delta\vec{p}(s)\right\}ds\,, \tag{9}$$

The beam section rotation is denoted by $\vec{p} = \theta\vec{e}_3$ and $\vec{q'} = \frac{d\vec{q}}{ds}$ is the displacement gradient.

The internal force and moment resultants involved in the virtual internal work are

$$\vec{R}^{(j)} \;=\; N^{(j)}\,\vec{\tau} + T^{(j)}\,\vec{n}\ , \tag{10a}$$

$$\vec{M}^{(j)} \;=\; M^{(j)}\,\vec{e}_3\ , \tag{10b}$$

In Eqn (10), $N^{(j)}$ is the axial force, $T^{(j)}$ is the shear force and $M^{(j)}$ is the bending moment in the $\vec{e}_3$ direction, for each beam section j.
It is worth mentioning that the internal work associated with the electric charge is zero since electric potential is imposed. Accordingly the electrostatic work does not appear in the virtual work Eqn (9).

2.4 Constitutive equations for the piezoelectric sandwich beam

The constitutive equations are derived from the classical linear beam theory and the piezoelectric material. The constitutive equations are written for the central elastic layer and for the piezoelectric sandwich section.
An equivalent single layer model neglecting the shear is based on the linear constitutive equations for the sandwich beam section. The piezoelectric sandwich beam model accounts for the transverse stress effect or the interaction between layers [Maurini et al., 2004].

a - For the elastic section $\mathcal{A}_1 \cup \mathcal{A}_3$, the constitutive equations for the axial force and the bending are

$$N^{(j)}(s) = K_{N\epsilon}^{(j)} \varepsilon(s) \qquad j = 1, 3\,, \tag{11a}$$

$$M_e^{(j)}(s) = K_{M\kappa}^{(j)} \kappa(s) \qquad j = 1, 3\,, \tag{11b}$$

where $K_{N\epsilon}^{(1)} = K_{N\epsilon}^{(3)}$ and $K_{M\kappa}^{(1)} = K_{M\kappa}^{(3)}$ are the extensional and bending stiffnesses, respectively. The detailed form of the coefficients depending on the beam parameters are given in Appendix A.

b - For the piezoelectric sandwich section $\mathcal{A}_2$, the constitutive equations are based on an improved layered piezoelectric beam model including the layer interaction or the effect of the transverse stress [Maurini et al., 2004].
Thanks to the material and geometrical symmetry of the piezoelectric sandwich beam there is only a coupling between the beam bending and the electric field (along the thickness direction). According to previous works [Fernandes and Pouget, 2010, Maurini et al., 2004], the constitutive equation takes on the following matrix form

$$\begin{bmatrix} N^{(2)} \\ M^{(2)} \\ \mathcal{Q} \end{bmatrix} = \begin{bmatrix} K_{N\epsilon}^{(2)} & 0 & 0 \\ 0 & K_{M\kappa}^{(2)} & K_{MV}^{(2)} \\ 0 & -K_{MV}^{(2)} & K_{\mathcal{Q}V}^{(2)} \end{bmatrix} \begin{bmatrix} \varepsilon \\ \kappa \\ V \end{bmatrix}. \tag{12}$$

The form of the coefficients are given in Appendix A as function of the material and geometrical parameters of the respective layers. In Eqn (12), $\mathcal{Q}$ denotes the total electric charge produced on the metallic electrodes.
From the bending moment given by the matrix of the constitutive equations Eqn (12), we split the bending moment as the sum of two terms

$$M^{(2)} = M_e^{(2)} + M_p\,. \tag{13}$$

The first part in Eqn (13) is the bending moment due to the elastic behavior while the second one can be interpreted as the piezoelectrically induced bending, being constitutively related to the

applied voltage on the electrodes of the piezoelectric layers. Consequently, we write

$$M_e^{(2)} = K_{M\kappa}^{(2)}\,\kappa\,, \tag{14a}$$

$$M_p = K_{MV}^{(2)}\,V\,. \tag{14b}$$

All the constitutive coefficients in Eqns (11) and (12) are given in Appendix A.

2.5 Dimensionless notations

We introduce the following rescaling for the lengths, forces, moment and energy

$$\begin{aligned} S =& \frac{s}{L_0}\,, \quad \vec{Q} = (X,Y) = \frac{\vec{q}}{L_0} = \left(\frac{x}{L_0}, \frac{y}{L_0}\right)\,, \quad \Delta\ell = \frac{\Delta L}{L_0}\,, \\ \vec{\bar{R}} =& \frac{\vec{R}}{R_0}\,, \quad \vec{\bar{M}} = \frac{\vec{M}}{M_0}\,, \quad \mathcal{W}_i = \frac{W_i}{W_0}\,, \end{aligned} \tag{15}$$

where the scaling reference parameters are given by $R_0 = E_e A_e k_e$, $M_0 = E_e I_e / L_0$ and $W_0 = R_0 L_0$. The key parameter is defined by $k_e = \frac{I_e}{A_e L_0^2}$, moreover $k_e \propto (h_e/L_0)^2$ where L_0/h_e is the slenderness ratio of the beam. It is worthwhile noting that all these dimensionless variables are defined with respect to the central elastic layer of the composite piezoelectric beam. Thanks to the above defined dimensionless variables, the non dimensional resultant takes on the form

$$\vec{\bar{R}}^{(j)} = \bar{N}^{(j)}\vec{\tau} + \bar{T}^{(j)}\vec{n}\,, \qquad j \in \{1,2,3\}\,, \tag{16}$$

we set $\bar{N}^{(j)} = N^{(j)}/R_0$ and $\bar{T}^{(j)} = T^{(j)}/R_0$.

3 Variational formulation and equations of the equilibrium

On using the dimensionless quantities previously introduced, the variation of the internal work can be recasted into

$$\delta\mathcal{W}_i = -\sum_{j=1}^{3}\int_{\mathcal{A}_j}\left\{\vec{\bar{R}}^{(j)}(S)\cdot\delta\vec{Q}_{,S} + \vec{\bar{M}}^{(j)}(S)\cdot\delta\vec{P}_{,S} - \Lambda\left(\vec{\tau}\times\vec{\bar{R}}^{(j)}(S)\right)\delta\vec{P}\right\}dS\,. \tag{17}$$

On accounting for Eqn (13), the variation of the internal work takes on the following form

$$\begin{aligned} \delta\mathcal{W}_i = -\sum_{j=1}^{3}\int_{\mathcal{A}_j}&\left\{\vec{\bar{R}}^{(j)}(S)\cdot\delta\vec{Q}_{,S} + \vec{\bar{M}}_e^{(j)}(S)\cdot\delta\vec{P}_{,S} - \Lambda\left(\vec{\tau}\times\vec{\bar{R}}^{(j)}((S)\right)\delta\vec{P}\right\}dS \\ &+ \bar{M}_p\vec{e}_3\cdot\delta\vec{P}\,(S_C) - \bar{M}_p\vec{e}_3\cdot\delta\vec{P}\,(S_D)\,. \end{aligned} \tag{18}$$

It is now clear that the bistable beam equipped with piezoelectric actuators can be seen as a buckled elastic beam subject to applied moments $-M_p\vec{e}_3$ and $+M_p\vec{e}_3$ respectively at the ends of the piezoelectric elements, namely at the curvilinear abscissa S_C and S_D as depicted in Figure 2. By means of an integration by part and accounting for the conditions at the beam ends, the variation of the internal work becomes

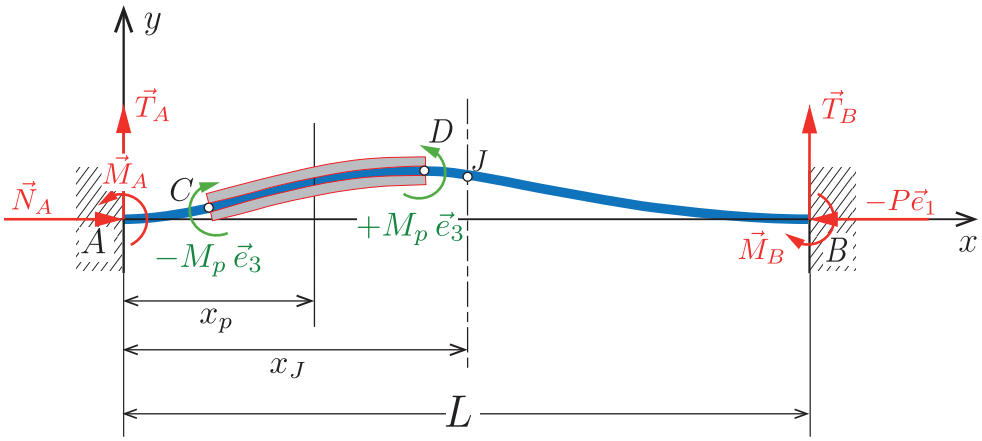

Figure 2: Actuation of the clamped-clamped elastic beam by a single pair of piezoelectric layers. Piezoelectrically induced moment applied at the ends C and D of the actuator and the forces and moments at the clamping ends A and B of the beam.

$$\begin{aligned}\delta\mathcal{W}_i = &\sum_{j=1}^{3}\int_{\mathcal{A}_j}\left\{\frac{d\vec{\bar{R}}^{(j)}}{dS}\cdot\delta\vec{Q}+\left(\frac{d\vec{\bar{M}}_e^{(j)}}{dS}+\Lambda\left(\vec{\tau}\times\vec{\bar{R}}^{(j)}\right)\right)\cdot\delta\vec{P}\right\}dS\\ &+[\![\vec{\bar{R}}]\!](S_C)\cdot\delta\vec{Q}\,(S_C)-[\![\vec{\bar{R}}]\!](S_D)\cdot\delta\vec{Q}\,(S_D)\\ &+\left\{[\![\vec{\bar{M}}_e]\!](S_C)+\bar{M}_p\vec{e}_3\right\}\cdot\delta\vec{P}\,(S_C)+\left\{[\![\vec{\bar{M}}_e]\!](S_D)-\bar{M}_p\vec{e}_3\right\}\cdot\delta\vec{P}\,(S_D)\ ,\end{aligned}\tag{19}$$

where $[\![-]\!]$ denotes the jump of a variable at the curvilinear points S_C or S_D of the deformed beam.

Now, we consider the variational equation Eqn (8) which must be satisfied for any arbitrary variations $\delta\vec{Q}$ and $\delta\vec{P}$ meeting the boundary conditions at $S=0$ and $S=1$ (clamped-clamped beam). We deduce the equations of the bistable beam

$$\frac{d\vec{\bar{R}}^{(j)}}{dS} = \vec{0} \qquad S\in[0,1]\ , \tag{20a}$$

$$\frac{d\vec{\bar{M}}_e^{(j)}}{dS}+\Lambda\left(\vec{\tau}\times\vec{\bar{R}}^{(j)}\right) = \vec{0} \qquad S\in\mathcal{A}_j \quad j=1,2,3\ , \tag{20b}$$

where the subscript j refers as to the beam sections $\mathcal{A}_1=[0,S_C[$, $\mathcal{A}_2=]S_C,S_D[$ and $\mathcal{A}_2=]S_D,1]$. Along with the above equations the associated jump conditions at the piezoelectric actuator ends are given by

$$[\![\vec{\bar{R}}]\!](S_C) = \vec{0}\,, \tag{21a}$$

$$[\![\vec{\bar{R}}]\!](S_D) = \vec{0}\,, \tag{21b}$$

$$[\![\vec{\bar{M}}_e]\!](S_C)+\bar{M}_p\vec{e}_3 = \vec{0}\,, \tag{21c}$$

$$[\![\vec{\bar{M}}_e]\!](S_D)-\bar{M}_p\vec{e}_3 = \vec{0}\,. \tag{21d}$$

The beam equations are completed by the constitutive equations for the bending moment and the resultant. The constitutive equations are precisely written for the three sections.

a - Section $\mathcal{A}_1 \cup \mathcal{A}_3$ (elastic layers). The constitutive equations for the extensional strain is

$$\varepsilon(S) = k_e \bar{N}^{(j)}(S) \qquad j \in \{1,3\}, \tag{22}$$

with k_e the extensibility parameter (see Appendix A for the definition according to the beam parameters). The bending moment is given by

$$\bar{M}_e^{(j)}(S) = \theta_{,S}(S) \qquad j \in \{1,3\}. \tag{23}$$

b - Section $\mathcal{A}_2$ (sandwich piezoelectric beam). The extensibility strain is

$$\varepsilon(S) = k_p \bar{N}^{(2)}(S), \tag{24}$$

where k_p is the extensibility modulus associated with the piezoelectric layers defined as follows

$$k_p = \left(\frac{K_{N\varepsilon}^{(1)}}{K_{N\varepsilon}^{(2)}}\right) k_e. \tag{25}$$

Referring to Eqn (14), the elastic part of the bending moment takes on the form

$$\bar{M}_e^{(2)} = \left(\frac{K_{M\kappa}^{(2)}}{K_{M\kappa}^{(1)}}\right) \theta_{,S}. \tag{26}$$

The piezoelectrically induced bending moment is given by

$$\bar{M}_p = \left(\frac{K_{MV}^{(2)}}{K_{M\kappa}^{(1)}}\right) V, \tag{27}$$

where V is the applied electric potential.
The total bending moment in the sandwich section is then the sum of the elastic bending moment Eqn (26) and the piezoelectrically induced moment Eqn (27).

According to Eqns (4), the geometrical relationships between the configurational parameters (X, Y, θ) are for the elastic sections

$$X_{,S} = \left(1 + k_e \bar{N}^{(j)}\right) \cos(\theta) \qquad j \in \{1,3\}, \tag{28a}$$

$$Y_{,S} = \left(1 + k_e \bar{N}^{(j)}\right) \sin(\theta) \qquad j \in \{1,3\}. \tag{28b}$$

For the piezoelectric sandwich zone, we have

$$X_{,S} = \left(1 + k_p \bar{N}^{(2)}\right) \cos(\theta), \tag{29a}$$

$$Y_{,S} = \left(1 + k_p \bar{N}^{(2)}\right) \sin(\theta). \tag{29b}$$

We now summarize the set of model equations that we have established. The equations of the buckled beam sandwiched by two piezoelectric layers are given by the differential equations Eqns (20). These equations are accompanied by the constitutive equations Eqns (22 to 27) for the axial force and bending moment according to the beam section considered. The conditions at the ends - namely points C and D - of the piezoelectric sandwich section are given by Eqns (21).

Going back to Eqn (20) along with Eqns (16, 23 and 26), the equilibrium equation takes the form

$$\theta'' + \bar{T} - \frac{1}{2}k_e\left(\bar{P}^2 - \bar{T}_A^2\right)\sin(2\theta) + k_e\bar{P}\bar{T}_A\cos(2\theta) = 0\,, \tag{30}$$

for the elastic sections ($S \in \mathcal{A}_1 \cup \mathcal{A}_3$) and

$$\theta'' + \frac{1}{\eta}\left[\bar{T} - \frac{1}{2}k_p\left(\bar{P}^2 - \bar{T}_A^2\right)\sin(2\theta) + k_p\bar{P}\bar{T}_A\cos(2\theta)\right] = 0\,, \tag{31}$$

for the piezoelectric sandwich part ($S \in \mathcal{A}_2$). We have set $\eta = \frac{K^{(2)}_{M\kappa}}{K^{(1)}_{M\kappa}}$, the ratio of the bending modulus of the sandwich layer to that of the elastic layer (see Appendix A for definitions). Moreover, the shear force (in dimensionless notation) is written as

$$\bar{T} = \bar{P}\sin(\theta) - \bar{T}_A\cos(\theta)\ . \tag{32}$$

4 Numerical study and bistable response

4.1 Sketch of the numerical method

This Section provides an extensive study of the response of the bistable beam subject to an electrical load. More precisely, we determine the bistable beam snap-through when a difference of electric potential is applied to the piezoelectric actuators. With this in mind, we solve the equilibrium equations of the bistable beam sandwiched by two piezoelectric layers. The equations to be considered are given by Eqn (30) and Eqn (31) along with Eqn (32). The conditions at the ends of the beam are those of the clamping at the points A and B, i.e., $X(0) = Y(0) = \theta(0) = 0$ and $X(1) = 1 - \Delta\ell,\ Y(1) = 0,\ \theta(1) = 0$ where $\Delta\ell$ is the imposed end-shortening at the right end. We use a shooting method to solve the second-order equations; here, we are faced with a boundary-value problem. The input parameters for the shooting algorithm are the clamping efforts at the end A, i.e. $\bar{M}_A = \theta'_A$ and $\bar{T}_A$. The targets or the objective parameters are the clamping conditions at B. In the solving process, we must account for jump conditions at the ends C and D of the piezoelectric actuators given by Eqns (21). Eqn (27) provides the piezoelectrically induced bending moment as a function of the electric potential V. The equilibrium equations are solved by incrementing the difference of electric potential V from zero to the value that triggers the switching of the bistable beam from one stable position (top or bottom) to the other one. Nevertheless, the present boundary value problem is not so trivial since we are faced with an unstable path of the solution while the beam is switching from one stable configuration to the other one.

In order to overcome any problem of the divergence of the numerical algorithm and the discrepancy of the equilibrium branch, we control the vertical displacement of the material point of the beam defined by the intersection of the deformed beam and the vertical line located at the mid-point of the beam ends A and B referred as J (see Figure 2). The curvilinear abscissa of the crossing point noted by S_J is such that $X(S_J) = X(1)/2$. The vertical displacement $Y_J = Y(S_J)$ is incremented step by step when it moves along the vertical lines while the beam switches. At each increment of Y_J, we compute the electric potential difference (via the moments piezoelectrically induced at the end of the pair of actuators) leading to the required configuration. With this approach, the coordinates of the point J, $(X(S_J),\ Y(S_J))$ become the input parameters while the electric potential V and the curvilinear abscissa S_J are now the shooting parameters of the problem. In summary, the response of the bistable beam, i.e., the electrical potential difference applied to the actuators as a

function of of the mid-point vertical displacement $Y_J = Y(S_J)$ is obtained by solving the present boundary value problem.

We first consider the configuration where the piezoelectric actuators are centered at the mid-point of the bistable beam. In a first step, we establish the deformation of the bistable beam in its equilibrium position when the actuators are subject to a zero electrical potential difference (piezoelectric layers short-circuited). However, the beam is subject to a shortening ΔL imposed by a compressive force $P\vec{e}_1$ applied along the beam axis at point B.
The bistable structure consists of a thin stainless steel strip of Young modulus $E_e = 207GPa$, length $L_0 = 200\,mm$, cross-section $b \times h_e = 10\,mm \times 0.2\,mm$. The piezoelectric actuators are made of piezoelectric ceramics of the PZT family (Lead Zirconate Titanate). The material constants for the elastic, piezoelectric and dielectric properties are provided by the manufacturer PI Ceramic® for PIC151 ceramics. The constants are reported in the Table 1 below. It should be noted that the piezoelectric ceramics possesses a hexagonal symmetry or it is transversally isotropic. The electric polarization is along the anisotropic axis.

C_{11}^E $[GPa]$	C_{13}^E $[GPa]$	C_{33}^E $[GPa]$	C_{12}^E $[GPa]$	C_{44}^E $[GPa]$	e_{21} $[C/m^2]$	e_{22} $[C/m^2]$	e_{16} $[C/m^2]$	ε_{11}^S $[nF/m]$	ε_{22}^S $[nF/m]$
107.65	63.124	100.45	63.854	19.624	-9.6	15.1	12	9.828	7.544

Table 1: Material constants for PZT-PIC151 piezoelectric ceramics for the numerical studies.

The length of the actuators (for both layers) is $L_p = 50\,mm$, the width is $b = 10\,mm$ and their thickness is $h_p = 0.2\,mm$. In the case of centered actuators, we have $x_C = 75\,mm$ and $x_D = 125\,mm$ so $x_p = 100\,mm$. Figure 3 shows the deformation of the bistable beam after an end-shortening of $\Delta L = 0.05$ or $0.1\,mm$ in physical dimension. The deformation is computed using two methods: (i) the shooting method as described above and (ii) the finite element method for the 3D model using quadratic piezoelectric elements (C3D20E) from the code library ABAQUS®. After studying convergence, we choose a mesh with 3 elements in the thickness of each layer to ensure a quadratic distribution of the electric field. The deformation of the bistable beam shown in Figure 3 has a flat in the center of the beam due to the rigidity of the trilayer and producing a decrease in curvature in the actuator region. The maximum deflection occurs at $x_m = 100\,mm$ and $y_m = 2.57\,mm$.
In a second step, we compute the deformation of the beam by incrementing Y_J the vertical coordinate of the deformed beam moving along the vertical located at the mid-point X_J from the stable position as defined above. The equations of the elastica beam are then solved by using the shooting method to obtain a new equilibrium such that $Y_J = Y(S_J)$. We deduce the punctual piezoelectrically induced moments acting at the ends of the actuators that produce this equilibrium. Finally, we deduce the associated electrical potential difference given by Eqn (14) or Eqn (27). Applying an electric potential from one stable position to another leads to the bistable response, i.e. electric potential as a function of deflection Y_J; which is depicted in Figure 4. In addition, a 3D finite element computation validates the results coming from the elastica model (red solid lines in the diagram in Figure 4). However, the FE computation is restricted to the stable zone of the diagram (black points on the curve). The FE computation is performed for an electrical potential control up to the value $V = V_{max}$ that triggers beam snap-through, whose value is $V_{max} = \pm 286\,V$.
Using the results of the numerical simulations, which allowed us to plot the response of the bistable beam actuated by a pair of piezoelectric elements, we can sketch the switching scenario of the bistable beam. (a) When the voltage is zero, the deformation of the beam corresponds to the first buckling mode (deflection of the buckled beam in Figure 3 inverted downwards), (b) by increasing

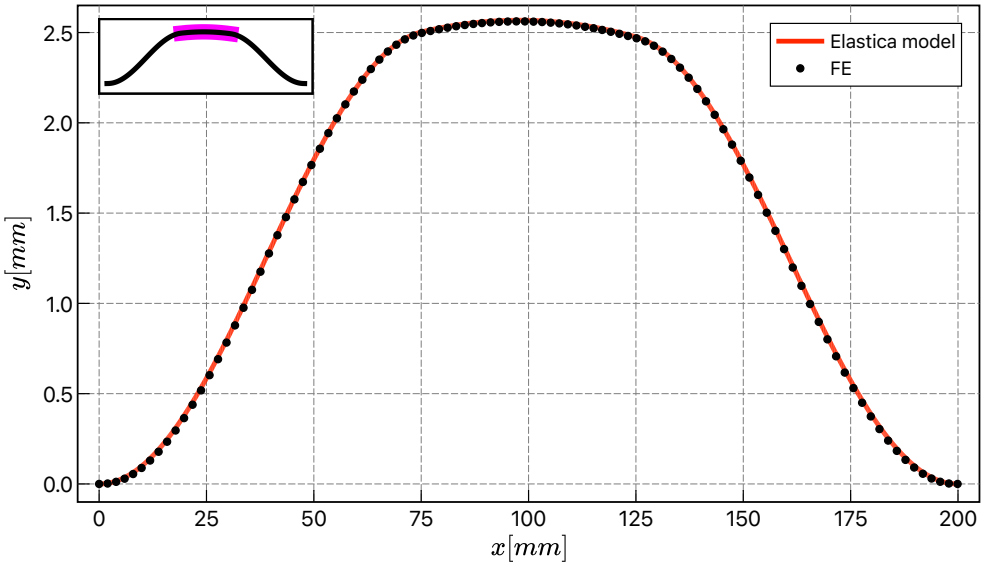

Figure 3: Deflection of the buckled beam sandwiched by a pair of piezoelectric layers (no electric load) for the mid-point actuator (in solid line : the elastica model, points : FE model) ($L_p = 50\,mm$, $X_p = x_p/L_0 = 0.5$, $h_p = 0.2\,mm$ and $\Delta\ell = 0.05\,\%$).

the electrical potential, the bistable deforms by essentially combining the first two buckling modes, (c) beyond V_{max}, the second buckling mode predominates and the bistable switches into the unstable region, (e) the electric potential is then reduced, passing through zero and then reaching the value $-V_{max}$, leading to a deformation similar to that in (b), but symmetrically reversed, and (f) after the electric potential is reset to zero, we find the first buckling mode again, but reversed. The scenario is repeated in the reversed way.

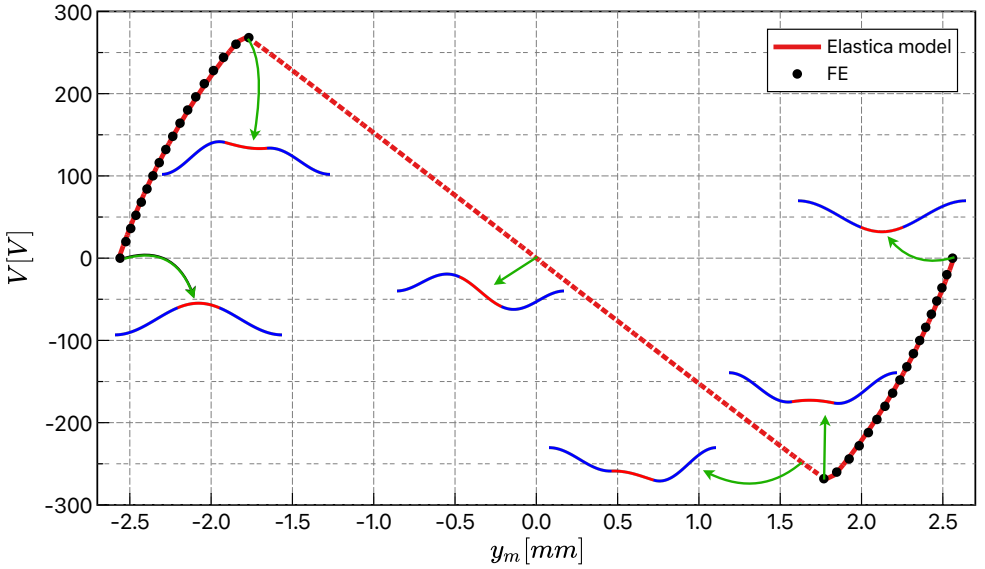

Figure 4: Bistable response : applied electric potential as function of the mid-point beam displacement for the centered piezoelectric actuator (solid line : elastica model (stable region), dashed line : elastica model (unstable region), points : FE model) ($L_p = 50\,mm$, $X_p = x_p/L_0 = 0.5$, $h_p = 0.2\,mm$ and $\Delta\ell = 0.05\,\%$).

We would like now to take a look at the influence of the actuator placement on the bistable response. We shift the piezoelectric actuators as close as possible to the left clamp, thus $x_p = 25\,mm$

($X_p = 0.125$). We repeat the solving method used for the actuators at the mid-point. First, we establish the deformation of the buckled beam without electrical loading. The results obtained from numerical simulations of the elastica model and from the finite element method are shown in Figure 5. The increase in bending stiffness due to the actuators placed close to the clamp point A produces a non-symmetrical deformation after buckling. In addition, the maximum deflection is $y_e = 2.65\,mm$ at $x_e = 119.25\,mm$, not at the mid-point of the beam.

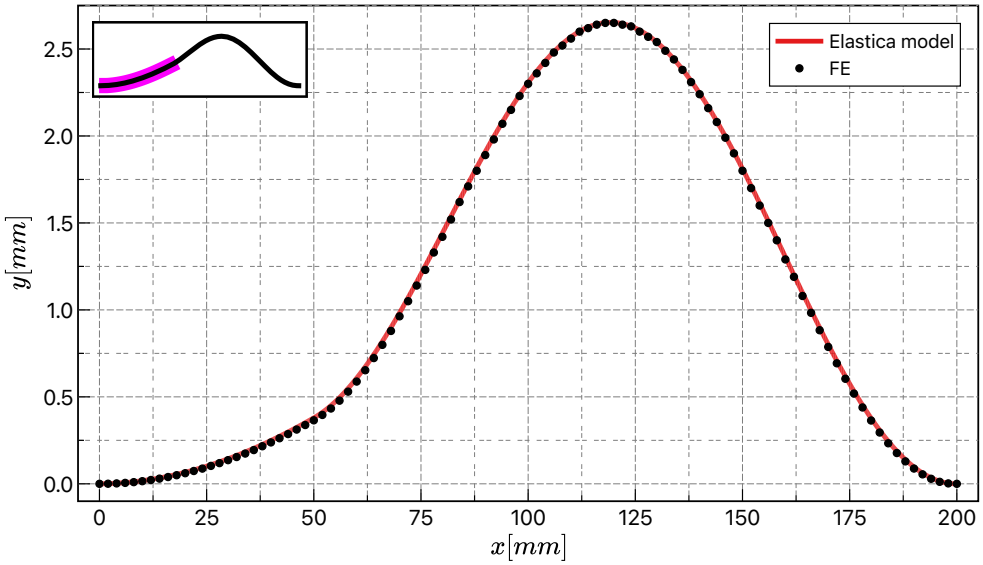

Figure 5: Deflection of the buckled beam sandwiched by a pair of piezoelectric layers (no electric load) for the off-center actuator (in solid line : the elastica model, points : FE model) ($L_p = 50\,mm$, $X_p = x_p/L_0 = 0.125$, $h_p = 0.2\,mm$ and $\Delta\ell = 0.05\,\%$).

As for the centered case, we study the response of the bistable beam during the switching when an electrical potential is applied to the piezoelectric actuators. In this configuration, the application of moments to the ends of the actuators is no longer symmetrical, the response will not be symmetrical as well when snap-through occurs from top to bottom or from bottom to top. This is illustrated in Figure 6. The results of elastica model simulations and the finite element method are superimposed on the figure. The FE results are limited to the regions of stability of the bistable beam response. In the bistable stability window, we have an excellent validation of the elastica model. The limit of the stability region stops at the value of the electric potential $V_{max} = \pm 139\,V$ that triggers the snap-through for both switching directions and the corresponding deflections is $y_J = \pm 0.18\,mm$. If we compare the configurations with centered and offset actuators, we see that, in the former case, the mid-point of the beam (the beam deflection measured along the vertical line at $X(1)/2$) moves 15.56 % of its total displacement before reaching the instability region, whereas this displacement is 46.6 % in the offset case. It is worth highlighting that by shifting the actuators close to the clamping point A (or clamp B), the applied electrical potential decreases by half compared with the centered case.

It would be interesting to say a few words about the role played by buckling modes during the snap-through transition. The deflections of the bistable beam are illustrated in Figure 6 at various key points during the switching process. Initially, with a zero electrical potential difference, the beam exhibits a deflection corresponding to its first buckling mode (downward). As the electrical potential decreases, it reaches a minimum value V_{max}, initiating the second mode switching. The bistable beam then switches and continues its travel until it reaches the upper stable position (buckling mode 1) when the electrical potential returns to zero. The transition from the upper

stable position to the lower one follows a different path due to the asymmetric configuration caused by the off-center actuators.

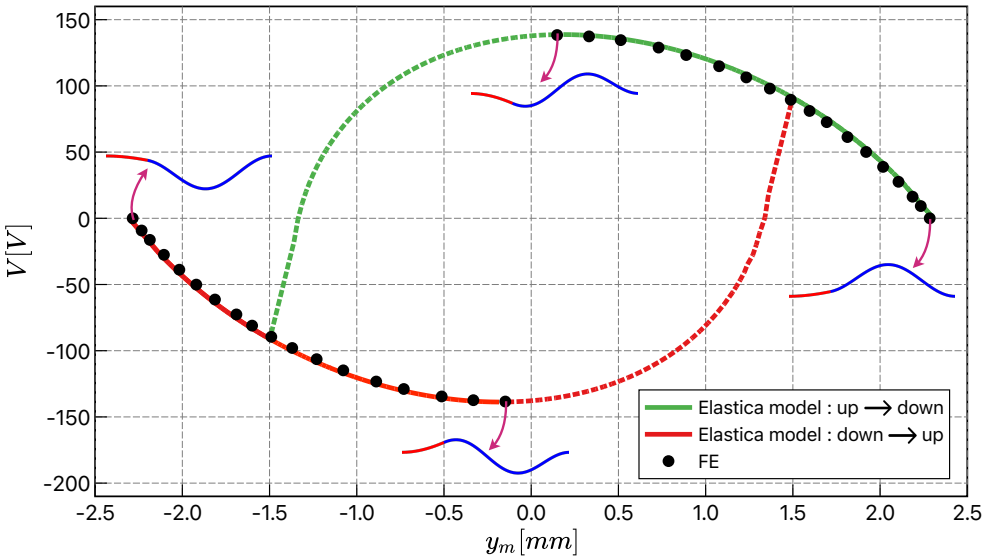

Figure 6: Bistable response : applied electric potential as function of the mid-point beam displacement for the off-center piezoelectric actuator (solid line : elastica model (stable region), dashed line : elastica model (unstable region), points : FE model, in green : switching from top to bottom, in red : switching from bottom to top)($L_p = 50\,mm$, $X_p = x_p/L_0 = 0.125$, $h_p = 0.2\,mm$ and $\Delta\ell = 0.05\,\%$).

4.2 Actuator optimization

Based on the two previous configurations (centered and offset actuators), we can ask the following question: are there an optimal actuator position and optimal dimensions of the actuators that minimize the applied electrical potential and maximize the bistable deflection of the bistable response? This section aims to answer this question. The optimization parameters to be identified are: (i) the optimal relative position of the actuators along the elastic beam, (ii) the length L_p of the actuators, and (iii) the relative thickness of the piezoelectric layers to that of the central elastic layer $\bar{h}_p = h_p/h_e$.

We first focus on the optimum position of the actuators. The other parameters are the length $L_p = 50\,mm$ and the thickness $h_p = 0.2\,mm$. For the given length of the actuators, the relative position X_p is in the range $[0.125, 0.875]$. The optimum position is computed using the elastica model; for each actuator position X_p, we compute the electrical potential V_{max} that drives the bistable to switch. This computation is carried out with the same spirit as that used to plot the voltage-displacement diagram for the centered actuators. The results of the simulations lead to the curve shown in Figure 7.

The variation of the electrical potential V_{max} as a function of the position of the piezoelectric actuators shows several interesting absolute and local minima. The V_{max} curve as a function of X_p displays two symmetrical absolute minima near the clamps A (or B), i.e. $X_p = 0.13$ (or $X_p = 0.87$) (see Figure 7). At this actuator position, the electric potential difference required to trigger the snap-through is $V_{max} = 133\,V$ is close to the clamps, the actuator must overcome the clamping moment, which restricts the rotation of the elastic beam. However, the moment at the opposite end

of the actuators induces a rotation of the beam section, triggering mode 2 buckling, which requires less energy compared to a symmetrical mode that would occur if the actuators were positioned at the center of the beam. The minima near the center of the beam correspond to positions slightly off-center, allowing for mode 2 (antisymmetric) buckling. At this point, we have a local minimum around $X_p = 0.476$ the associated voltage is $V_{max} = 179\,V$. In contrast, mode 3 (symmetric) buckling would be initiated, if the actuators were centered.

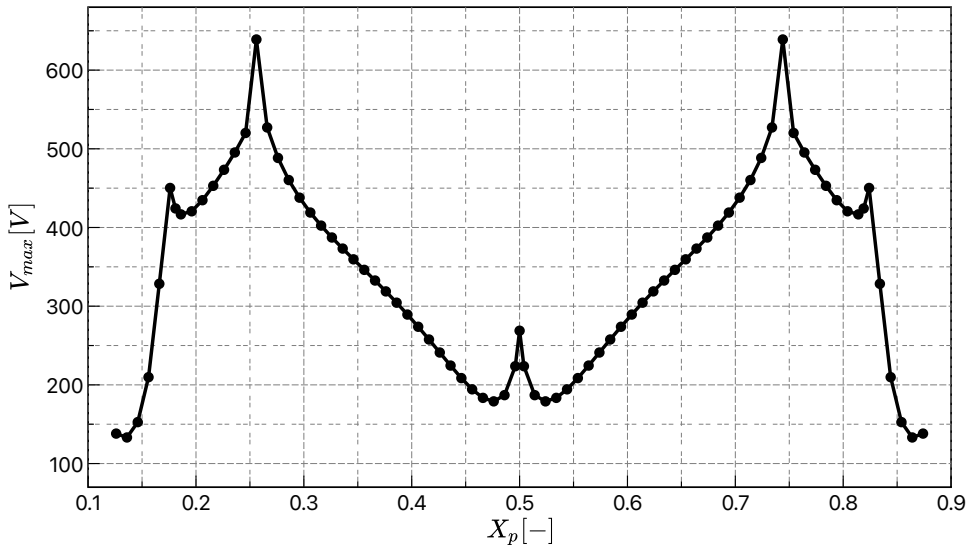

Figure 7: Optimization of the piezoelectric actuator location : maximum of the electric potential that triggers the bistable snap-through as function of the relative actuator position X_p ($L_p = 50\,mm$, $h_p = 0.2\,mm$ and $\Delta\ell = 0.05\,\%$).

In the second phase of the optimization, we examine the influence of actuator length L_p on the value of V_{max}. At this end, we place the actuator at the left end of the beam. Obviously, the length of the piezoelectric layers must be less than half the length of the beam. Numerical simulations show that there can be no snap-through for $\bar{L}_p < 0.05$ (actuators too short), where $\bar{L}_p = L_p/L_0$ defines the relative actuator length. The results of the actuator length optimization are shown in Figure 8. We note that the variation of V_{max} as a function of L_p is not monotonic. The switching voltage starts from a maximum at $L_p = 0.05$ (very short actuators) reaches a minimum at $L_p = 0.35$, and then increases slowly. We might think that longer piezoelectric actuators would allow a punctual bending moment to be applied further away from the clamping point A, thereby increasing its impact on the buckling mode two. However, by increasing the length of the actuator, the bending stiffness of the beam in the region of the piezoelectric layers is consequently increased. There is a trade-off between maximizing the action of piezoelectrically induced bending moments and minimizing bending stiffness in the tri-layer region. The optimal actuator length that balances the two constraints is $L_p = 0.35 \times L_0 = 70\,mm$.

The final optimization parameter is the thickness of the piezoelectric layers (let us remember that they are identical for both layers). We choose a configuration of the piezoelectric actuators of length $L_p = 70\,mm$ located close to the left end of the bistable beam. We increment the thickness $\bar{h}_p$ (relative thickness) of the piezoelectric layers over the interval $[0.01, 2]$. We run numerical simulations using the elastica model, and for each value of $\bar{h}_p$, we compute the electrical potential difference V_{max} that triggers snap-through. The results are shown in Figure 9, V_{max} as a function of $\bar{h}_p$. We can observe that the curve in Figure 9 has an absolute minimum for $\bar{h}_p = 0.95$; for this

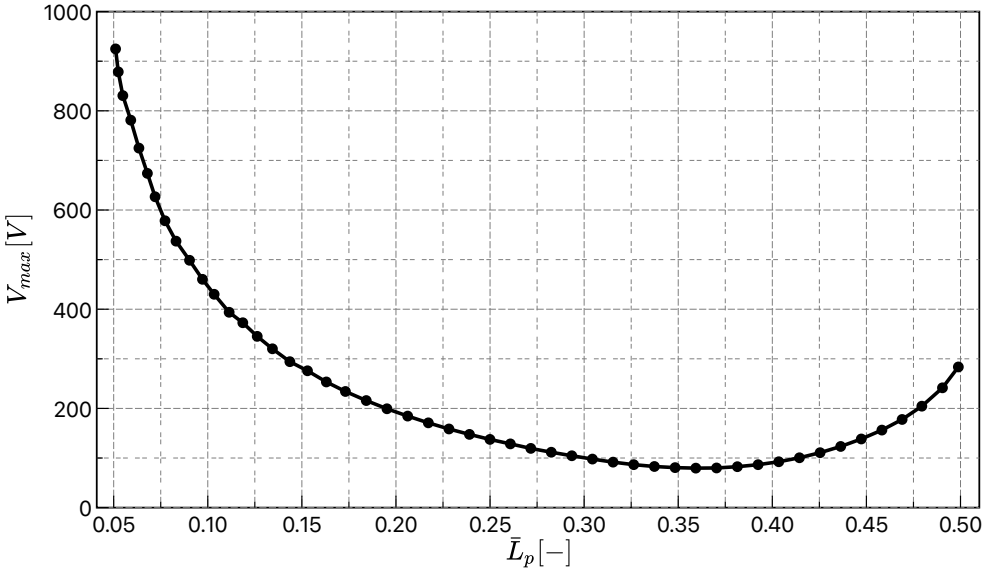

Figure 8: Optimization of the piezoelectric actuator length : maximum of the electric potential that triggers the bistable snap-through as function of the relative actuator length $\bar{L}_p$ ($x_p = L_p/2$, $h_p = 0.2\,mm$ and $\Delta\ell = 0.05\,\%$, the actuator is located at the left end of the beam).

value, the electric potential reaches the value $V_{max} = 78\,V$.
We note that the curve possesses a singular point at about $\bar{h}_p = 0.25$. This calls for in-depth discussions. The piezoelectric actuators increase the stiffness of the elastic beam in the interval $[X_p - L_p/2, X_p + L_p/2]$. However, the behavior of these piezoelectric elements generates moments at the ends of the actuators, which facilitate bistable switching. Therefore, there is a trade-off between the stiffness provided by the actuators and their action. In cases where the piezoelectric layers are relatively thin, the stiffness can be significantly offset by the moments induced by the piezoelectric elements. The lever arm associated with this moment, which can be approximated as $(h_p + h_e)/2$, tends to be small in such situations. There is a threshold value of $\bar{h}_p$, approximately 0.25 (see Fig.9), beyond which the additional stiffness becomes significant. However, at this point, the effect of this increased stiffness on counteracting switching is balanced out by larger actuation moments. Ultimately, the ideal compromise is characterized by a value of $\bar{h}_p$ that minimizes V_{max}, the threshold voltage that triggers the snap-through action.

As a conclusion of this optimization study, the most favorable configuration that leads to the minimum electrical potential to be applied to the piezoelectric layers to start snap-through is obtained for (i) the piezoelectric actuator length $\bar{L}_p = 0.35$ ($L_p = 70\,mm$), (ii) the thickness $\bar{h}_p = 0.95$ ($h_p \approx h_e$) and (iii) when the pair of the piezoelectric actuators is located close to either clamp of the beam, that is at $x_p = L_p/2$ (or $L_0 - L_p/2$).

4.3 Bistable actuation by means of two pairs of piezoelectric layers

In the case of actuation by just one pair of piezoelectric layers, we have an optimum configuration that does not ensure symmetry during the switching process. Moreover, the maximum beam deflection does not match that of the beam mid-point. For the majority of applications, it is more appropriate to obtain a symmetrical deformation of the beam. In this section, we focus on the response of the bistable equipped with two pairs of piezoelectric actuators subject to identical electrical potential differences. The actuator pairs are positioned symmetrically close to the clamping

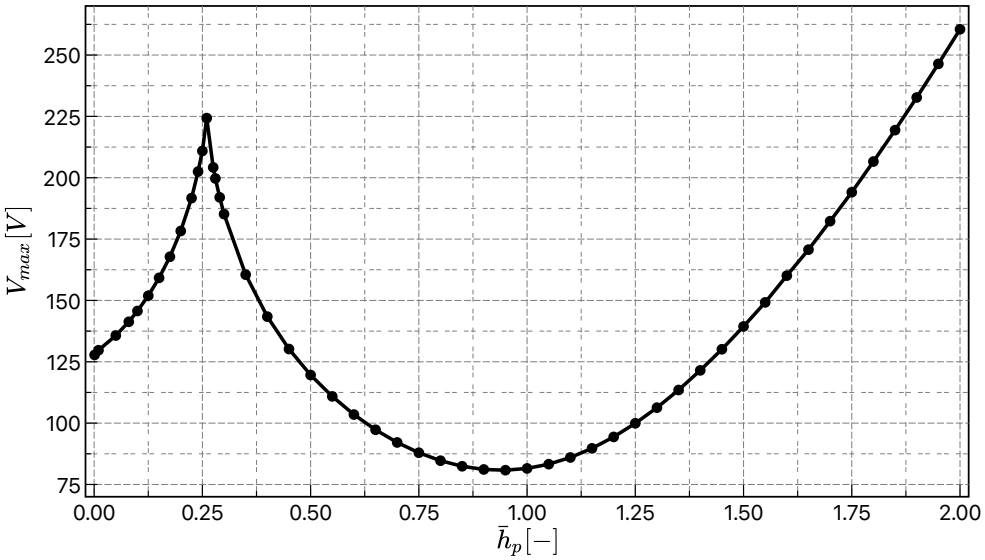

Figure 9: Optimization of the piezoelectric actuator thickness : maximum of the electric potential that triggers the bistable snap-through as function of the piezoelectric layer relative thickness $\bar{h}_p$ ($x_p/L_0 = 0.175$, $L_p = 70\,mm$ and $\Delta\ell = 0.05\,\%$, the actuator is located at the left end of the beam).

points A and B. In addition, the axes of electrical polarization of the 2 pairs are oriented in the same way along the thickness direction of the piezoelectric layers. Thus, we take $x_{p_1} = 35\,mm$ and $x_{p_2} = 165\,mm$, respectively for the first pair of actuators and for the second one. Figure 10 shows the beam equipped with two pairs of actuators exhibiting the geometrical parameters.

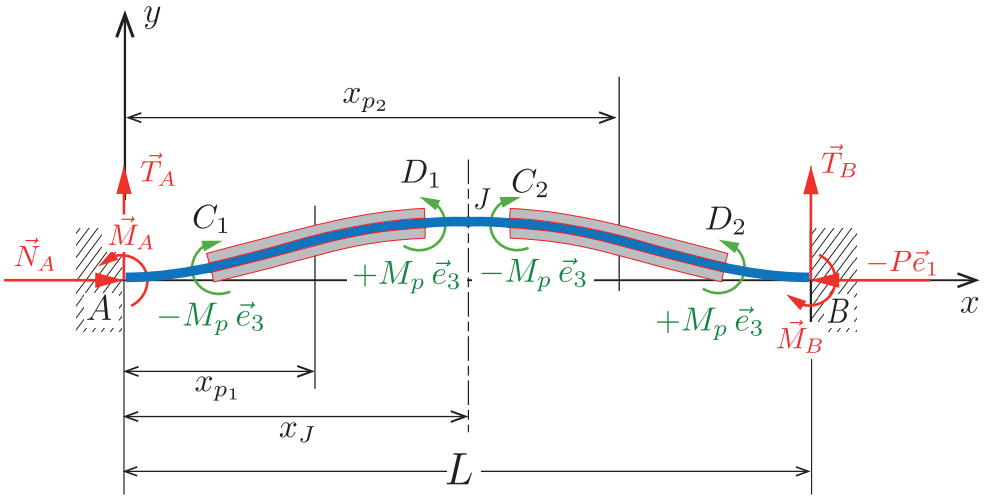

Figure 10: Actuation of the clamped-clamped elastic beam by two pairs of piezoelectric layers.

For this situation, we must adapt the system of the differential equations of the bistable beam, accounting for that the equations are then solved over 5 intervals, namely, $[A, C_1[$, $]C_1, D_1[$, $]D_1, C_2[$, $]C_2, D_2[$, and $]D_2, B]$, where the points C_1 and D_1 are the ends of the first actuator (close to the clamping point A) and C_2 and D_2 are the ends of the second actuator (close to the clamping point B). We compute the beam deformation subject to an end-shortening at point B, the electrical potential being set to zero. The deformation is shown in Figure 11 and compared with that of the beam equipped with only one pair of actuators. We note an increase of 4.8 % in beam deflection in favor of the beam equipped with 2 pairs of actuators. The approach is identical to that for

the case of a beam equipped with a single pair of actuators; especially, the control of the vertical displacement of the mid-point beam is an input parameter.

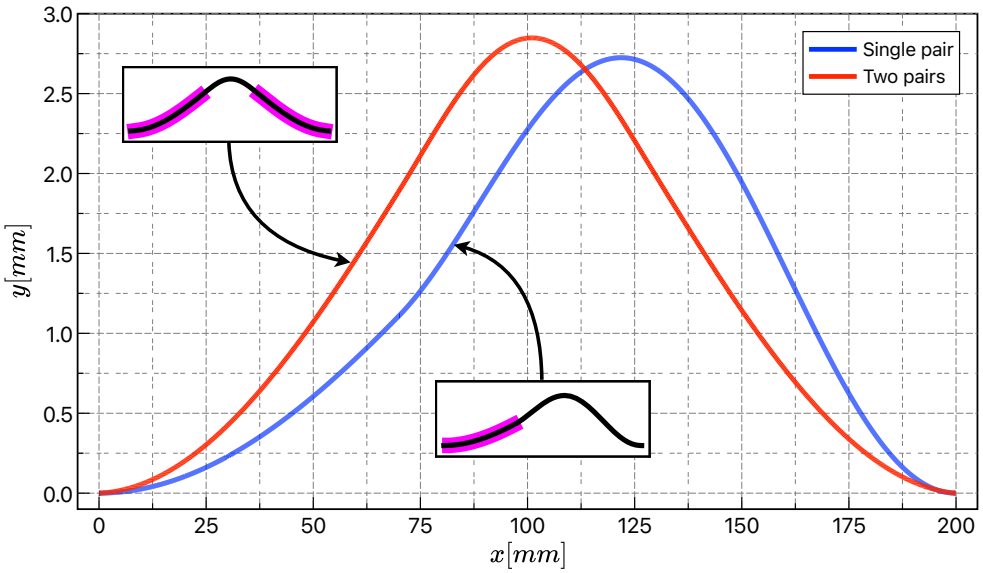

Figure 11: Deflection of the buckled beam sandwiched by two pairs of piezoelectric layers (no electric load) symmetrically placed with respect to the mid-point beam (red solid line). Comparison with the case of a single pair of piezoelectric layers (blue solid line) ($L_p = 70\,mm$, $h_p = 0.19\,mm$, and $\Delta\ell = 0.05\,\%$).

Figure 12 shows the snap-through diagram for the bistable beam, where the electrical potential difference applied to the actuators is a function of the deflection at the center of the beam. The curves obtained are compared to those obtained for the actuation by a single pair of piezoelectric elements.
Similarly to the studies of the switching of the bistable beam, either equipped with a centered pair of piezoelectric actuators (Figure 4) or with an offset pair of actuators (Figure 6), the bistable beam in its deformed state is plotted at key points of the bistable response curve V_{max} as a function of the vertical displacement of the center of the beam.

The above comparison allows us to draw the following conclusions :
(i) an increase of 24 % in the maximum beam deflection, despite the additional bending stiffness of the beam due to the actuators.
(ii) reduction of 12 % in the electrical potential difference producing snap-through.
(iii) snap-through paths in both directions (top to bottom and vice versa) are superimposed, in contrast to the case of a single pair of actuators.
This configuration - a bistable beam actuated by two pairs of piezoelectric elements - provides the optimum for greater switching while reducing loading, which makes this configuration more attractive for innovative applications in the MEMS field, for instance.

5 Conclusions

In the present work, we studied the bistable snap-through using piezoelectric actuators. Especially, the emphasis is placed on the bistable response, the maximal deflection, as function of the electric potential difference applied to the piezoelectric actuators. Based on the Elastica theory of elastic beams, the present research focuses on modeling of a bistable beam subject to buckling load. The

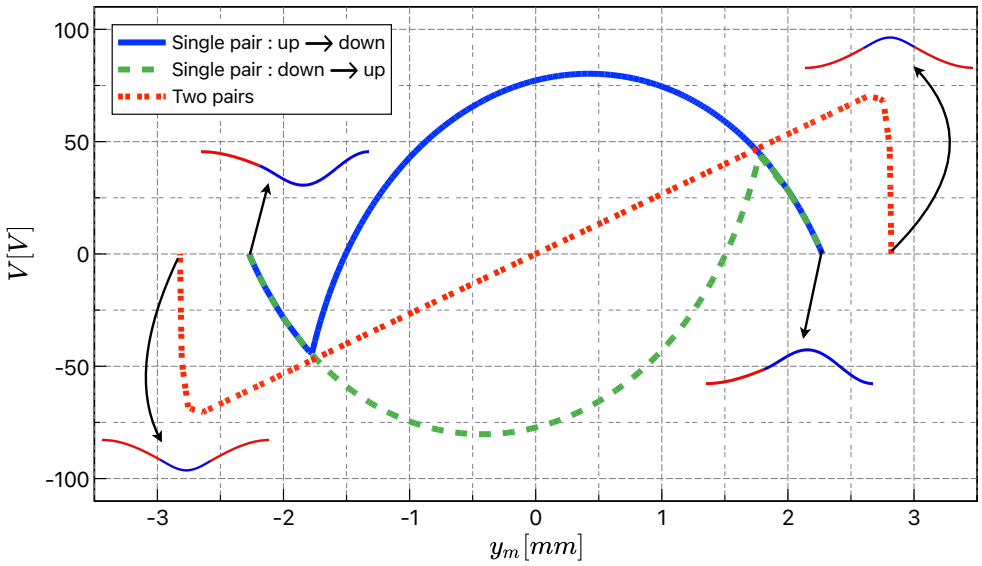

Figure 12: Bistable response : applied electric potential as function of the mid-point beam displacement by means of two pairs piezoelectric actuators (mixed broken red lines). Comparison with the case of a single pair of piezoelectric layers (blue solid line : single pair (switching from top to bottom), green dashed line : single pair (switching from bottom to top)) ($L_p = 70\,mm$, $h_p = 0.19\,mm$ and $\Delta\ell = 0.05\,\%$).

model accounts for the extensibility of the beam, which plays an essential role in the switching process. The bending effects of the bistable buckled beam are due to the action of the moments applied to the ends of the piezoelectric actuators. Furthermore, it is shown that the moments are directly related to the electrical potential difference applied to the piezoelectric layers by electromechanical coupling. We derive the equilibrium equations accounting for the piezoelectric sandwich section from a variational formulation of the piezoelectric beam.

We use a numerical algorithm for boundary value problems of the shooting method type to study the response of the bistable beam undergoing the action of an electric potential difference applied to the piezoelectric layers. The bistable response is characterized by the diagram of the voltage versus deflection of the beam midpoint. The results were validated using a finite element analysis. Two situations have been studied: (i) centered piezoelectric actuators and (ii) off-centered actuators. In the latter case, it is shown that the voltage required to trigger the bistable snap-through ($139\,V$) is lower than the voltage necessary for the centered case ($285\,V$).

An optimization study of the actuators proved to be indispensable in order to find the placement and the dimensions of the actuators that would lead to the maximum deflection for a minimum threshold of the electrical potential difference. The analysis led to a favorable configuration with (i) a relative length of the piezoelectric layers of $\bar{L}_p = 0.35$ (35 % of the total length of the beam) (see Figure 8), (ii) a thickness of the piezoelectric layers of the same order of magnitude as that of the central elastic layer (see Figure 9), and (iii) a position close to one or other of the beam ends (see Figure 7).

In the last part of the work, we have addressed the problem of the bistable actuation of a beam by means of two pairs of identical piezoelectric layers arranged in a sandwich configuration. In this case, we observe an increase in the mid-point deflection of the beam, in spite of an increase in the bending stiffness of the piezoelectric layers, and a decrease in the electrical potential difference that triggers the bistable snap-through.

The numerical study proposed in sub-section 4.2 shows the effectiveness of the bistable buckled beam actuated by piezoelectric elements. More precisely, for a beam $20\,cm$ long with a thickness of $0.2\,mm$ partly sandwiched by piezoelectric layers $7\,cm$ long a deflection of the order of a couple of millimeters is obtained using a voltage less than $100\,V$. A natural extension is the realization of a demonstration prototype. The use of the Micro Fiber Composite layers made of piezoelectric fibers embedded in a soft epoxy matrix and covered by interdigitated electrodes appears the suitable material for rather large beam deflection with reasonable voltage of around $100\,V$. The piezoelectric actuation of shallow elastic arches is also an interesting extension of the present work. At last, the modeling and results reported in the study can be an attractive interest in engineering applications such as Micro-Electro-Mechanical Systems.

Appendix A Constitutive coefficients for the sandwich piezoelectric beam

The appendix focuses on the explicit expressions for the piezoelectric beam constitutive coefficients based on an improved Euler-Bernoulli model of piezoelectric laminates including the 3D effects. The model accounts for the influence of the interaction between the different layers and sectional bending and extension in the transverse direction. The piezoelectric beam constitutive coefficients are deduced from the reduction of a piezoelectric multilayer plate (2D) based on the standard Love-Kirchhoff model to a 1D model by assuming vanishing the transverse stress resultant and moment [Fernandes and Pouget, 2010, Maurini et al., 2004].

Let us consider a three-layered plate made of a purely elastic layer (thickness h_e, $E_e = 207GPa$; $\nu_e = 0.3$) sandwiched with two piezoelectric PZT-PIC151 ceramics (thickness h_p). The top and bottom faces of both piezoelectric layers are recovered with conducting electrodes as depicted in Figure 1.a. It is assumed that each layer is materially homogeneous with constant thickness. The piezoelectric layers are supposed to be transversely isotropic with respect to the poling axis oriented along the thickness direction (direction 2). The plate kinematics is based on the standard Love-Kirchhoff hypotheses. In addition, the through-thickness variation of the electric potential is taken as a quadratic function of the thickness coordinate. Then, we have

$$\left\{\begin{array}{l} u_\alpha\left(x,y,z\right) = u_\alpha^0\left(x,z\right) - y w_{,\alpha}\left(x,z\right)\,, \\ u_3\left(x,y,z\right) = w\left(x,z\right)\,, \\ \phi_{(p_1,p_2)}\left(x,y,z\right) = \phi_{(p_1,p_2)}^{(0)}\left(x,z\right) + y\phi_{(p_1,p_2)}^{(1)}\left(x,z\right) + y^2\phi_{(p_1,p_2)}^{(2)}\left(x,z\right)\,. \end{array}\right. \tag{A.1}$$

Using the Voigt notation, the components of the strain tensor for the Love-Kirchhoff plate theory are :

$$S_\alpha = \varepsilon_\alpha - y\,\kappa_\alpha \qquad \alpha = 1,3 \tag{A.2}$$

with

$$\varepsilon_\alpha = u_{\alpha,\alpha}^0 \quad \text{and} \quad \kappa_\alpha = w_{,\alpha\alpha}\,. \tag{A.3}$$

The piezoelectric constitutive equations for the piezoelectric layers are given by (see [Ikeda, 1990], using Voigt notation)

$$\left\{\begin{array}{l} \sigma_\alpha = C_{\alpha\beta}^E S_\beta - e_{i\alpha}E_i\,, \\ D_i = e_{i\beta}S_\beta + \epsilon_{ij}^S E_j\,, \end{array}\right. \tag{A.4}$$

where $C_{\alpha\beta}^E$, $e_{i\alpha}$, and ϵ_{ij}^S are the components of the elastic modulus matrix at a given electric field, the components of the piezoelectric coupling matrice and the components of the dielectric

coefficient matrice at a given deformation, respectively.
We assume the hypothesis of thin elastic plate which states that the transverse normal stress σ_2 and the shear stresses can be neglected with respect to the other stress components. The new piezoelectric constitutive laws are given by :

$$\left\{\begin{array}{lcl} \sigma_1 &=& \bar{c}_{11}S_1 + \bar{c}_{13}S_3 + \bar{e}_{21}\phi_{,y}\,, \\ \sigma_3 &=& \bar{c}_{13}S_1 + \bar{c}_{11}S_3 + \bar{e}_{21}\phi_{,y}\,, \\ D_2 &=& \bar{e}_{21}S_1 + \bar{e}_{21}S_3 - \bar{\epsilon}_{22}\phi_{,y}\,, \end{array}\right. \tag{A.5}$$

with

$$\left\{\begin{array}{lcl} \bar{c}_{1\alpha} &=& c_{1\alpha}^E - \dfrac{{c_{12}^E}^2}{c_{22}^E}\,, \\ \bar{e}_{21} &=& e_{21} - \dfrac{c_{12}^E}{c_{22}^E}e_{22}\,, \\ \bar{\epsilon}_{22} &=& \epsilon_{22}^S + \dfrac{{e_{22}}^2}{c_{22}^E}\,. \end{array}\right. \tag{A.6}$$

Accounting for the electric boundary and continuity conditions, the electric potential for the two layers can be written as

$$\phi_{p_1}(y) = \left(y - \frac{h_e}{2}\right)\left[\frac{V}{h_p} - \frac{1}{2}\left(y - \frac{h_t}{2}\right)\frac{\bar{e}_{21}}{\bar{\epsilon}_{22}}\left(\kappa_1 + \kappa_3\right)\right]\,, \tag{A.7}$$

$$\phi_{p_2}(y) = -\left(y - \frac{h_e}{2}\right)\left[\frac{V}{h_p} + \frac{1}{2}\left(y - \frac{h_t}{2}\right)\frac{\bar{e}_{21}}{\bar{\epsilon}_{22}}\left(\kappa_1 + \kappa_3\right)\right]\,. \tag{A.8}$$

The constitutive equations for the sandwich plate take on the form

$$\left\{\begin{array}{lcl} M_1 &=& -\displaystyle\int_{-b/2}^{b/2}\int_{-h_t/2}^{h_t/2} y\sigma_3(x,y,z)\,dydz\,, \\ M_3 &=& -\displaystyle\int_{-b/2}^{b/2}\int_{-h_t/2}^{h_t/2} y\sigma_1(x,y,z)\,dydz\,, \\ \mathcal{Q} &=& -\displaystyle\int_{-b/2}^{b/2}\int_{-h_t/2}^{h_t/2} D_2(x,y,z)\,dydz\,, \end{array}\right. \tag{A.9}$$

where M_1 and M_3 are respectively the flexural moments around directions 1 and 3 and $\mathcal{Q}$ is the global electric charge on the piezoelectric layer surfaces.

After integration, we can easily find :

$$\left[\begin{array}{c} M_1 \\ M_3 \\ \mathcal{Q} \end{array}\right] = \left[\begin{array}{ccc} K_{11} & K_{13} & F_1 \\ K_{13} & K_{11} & F_1 \\ -F_1 & -F_1 & G \end{array}\right]\left[\begin{array}{c} \kappa_1 \\ \kappa_3 \\ V \end{array}\right] \tag{A.10}$$

with

$$K_{1\alpha} = \frac{bh_p}{2}(h_e + h_p)^2\,\bar{c}_{1\alpha}^{(p)} + 2I_p\,(\bar{c}_{1\alpha}^{(p)} + \hat{c}_{1\alpha}^{(p)}) + I_e\,\bar{c}_{1\alpha}^{(e)} \quad \alpha = 1,3 \qquad \text{where} \qquad \hat{c}_{1\alpha}^{(p)} = \bar{c}_{1\alpha}^{(p)} + \frac{\bar{e}_{21}^2}{\bar{\epsilon}_{22}}\,,$$

$$F_1 = -b(h_e + h_p)\,\bar{e}_{21} \qquad \text{and} \qquad G = \frac{2b}{h_p}\bar{\epsilon}_{22}\,.$$

By assuming a vanishing transverse resultant of stress moment $M_1 = 0$, we are able to reduce the constitutive equations to that of the beam. The latter take on the form

$$\begin{bmatrix} M_3 \\ \mathcal{Q} \end{bmatrix} = \begin{bmatrix} K_{M\kappa} & K_{MV} \\ -K_{MV} & K_{\mathcal{Q}V} \end{bmatrix} \begin{bmatrix} \kappa_3 \\ V \end{bmatrix} \tag{A.11}$$

with

$$K_{M\kappa} = K_{11} - \frac{K_{13}^2}{K_{11}}; \quad K_{MV} = F_1 \left(1 - \frac{K_{13}}{K_{11}}\right) \quad \text{and} \quad K_{\mathcal{Q}V} = G + \frac{F_1^2}{K_{11}} \, .$$

In addition to the coupling bending-electric potential constitutive equations given by Eqn (A.11), we must account for the extensional behavior of the piezoelectric sandwich beam. Due to the symmetry of the problem, there is no coupling between the beam stretching and bending. Consequently, the constitutive equation for the beam stretching is written as follow

$$N^{(2)} = K_{N\epsilon}^{(2)} \varepsilon \, , \tag{A.12}$$

where the effective extensibility modulus is $K_{N\epsilon}^{(2)} = A_e E_e + 2A_p E_p$, the corresponding Young modulus are $E_e = \bar{c}_{11}^{(e)}$ and $E_p = \bar{c}_{11}^{(p)}$ for the elastic and piezoelectric layers, respectively. We have A_e the section area of the elastic layer and A_p that of the piezoelectric layer.

We must consider the constitutive equations for the purely elastic layer (sections $\mathcal{A}_1$ and $\mathcal{A}_3$). Their expressions are reduced to

$$N^{(1)} = K_{N\epsilon}^{(1)} \, \varepsilon \, , \tag{A.13a}$$

$$M^{(1)} = K_{M\kappa}^{(1)} \, \kappa \, . \tag{A.13b}$$

In the above equations $K_{N\epsilon}^{(1)} = A_e E_e$ is the extensional modulus, and $K_{M\kappa}^{(1)} = I_e E_e$ the bending modulus where I_e is the quadratic moment of the beam section.
To make the article easier to read, we will set $M_3 = M$ and $\kappa_3 = \kappa$ in the article body.

Acknowledgements

The research work reported in the paper has been supported by the research project BISCELTECH funded by Fonds Unique Interministériel (FUI-APP21).

References

A. Abbasi, T. G. Sano, D. Yan, and P. M. Reis. Snap buckling of bistable beams under combined mechanical and magnetic loading. *Philosophical Transactions of the Royal Society A: Mathematical, Physical and Engineering Sciences*, 381(2244):20220029, 2023. doi: 10.1098/rsta.2022.0029. URL `https://royalsocietypublishing.org/doi/abs/10.1098/rsta.2022.0029`.

S. Aimmanee and K. Tichakorn. *Piezoelectrically induced snap-through buckling in a buckled beam bonded with a segmented actuator.* Journal of Intelligent Material Systems and Structures, 2018. doi: 10.1177/1045389X17754270.

A. Amor, A. Fernandes, and J. Pouget. Snap-through of elastic bistable beam under contactless magnetic actuation. *International Journal of Non-Linear Mechanics*, 119:103358, 2020. ISSN 0020-7462. doi: https://doi.org/10.1016/j.ijnonlinmec.2019.103358. URL `https://www.sciencedirect.com/science/article/pii/S0020746219305347`.

A. Amor, A. Fernandes, and J. Pouget. Numerical and experimental investigations of bistable beam snapping using distributed laplace force. *Meccanica*, 57(1):109–119, Jan 2022. ISSN 1572-9648. doi: 10.1007/s11012-021-01412-5. URL https://doi.org/10.1007/s11012-021-01412-5.

P. Anilkumar, A. Haldar, E. Jansen, B. Rao, and R. Rolfes. Snap-through of bistable variable stiffness laminates using mfc actuators. *Composite Structures*, 266:113694, 2021. ISSN 0263-8223. doi: https://doi.org/10.1016/j.compstruct.2021.113694. URL https://www.sciencedirect.com/science/article/pii/S0263822321001550.

S. R. Anton and H. A. Sodano. A review of power harvesting using piezoelectric materials (2003â2006). *Smart Materials and Structures*, 16(3):R1, may 2007. doi: 10.1088/0964-1726/16/3/R01. URL https://dx.doi.org/10.1088/0964-1726/16/3/R01.

J. Barth, B. Krevet, and M. Kohl. A bistable shape memory microswitch with high energy density. *Smart Materials and Structures*, 19(9):094004, aug 2010. doi: 10.1088/0964-1726/19/9/094004. URL https://doi.org/10.1088/0964-1726/19/9/094004.

Z. Bažant, L. Cedolin, and Z. Bazant. *Stability of Structures: Elastic, Inelastic, Fracture and Damage Theories*. Oxford University Press, 1991.

D. Bigoni. *Nonlinear Solid Mechanics: Bifurcation Theory and Material Instability*. Cambridge University Press, 2012.

C. R. Bowen, P. F. Giddings, A. I. Salo, and H. A. Kim. Modeling and characterization of piezoelectrically actuated bistable composites. *IEEE Transactions on Ultrasonics, Ferroelectrics, and Frequency Control*, 58(9):1737–1750, 2011. doi: 10.1109/TUFFC.2011.2011.

B. Camescasse, A. Fernandes, and J. Pouget. Bistable buckled beam: Elastica modeling and analysis of static actuation. *International Journal of Solids and Structures*, 50(19): 2881–2893, 2013. ISSN 0020-7683. doi: https://doi.org/10.1016/j.ijsolstr.2013.05.005. URL https://www.sciencedirect.com/science/article/pii/S0020768313001972.

Y. Cao, M. Derakhshani, Y. Fang, G. Huang, and C. Cao. Bistable structures for advanced functional systems. *Advanced Functional Materials*, 31 (45):2106231, 2021. doi: https://doi.org/10.1002/adfm.202106231. URL https://onlinelibrary.wiley.com/doi/abs/10.1002/adfm.202106231.

P. Cazottes, A. Fernandes, J. Pouget, and M. Hafez. Bistable Buckled Beam: Modeling of Actuating Force and Experimental Validations. *Journal of Mechanical Design*, 131(10), 09 2009. ISSN 1050-0472. doi: 10.1115/1.3179003. URL https://doi.org/10.1115/1.3179003. 101001.

B. Charlot, W. Sun, K. Yamashita, H. Fujita, and H. Toshiyoshi. Bistable nanowire for micromechanical memory. *Journal of Micromechanics and Microengineering*, 18(4):045005, feb 2008. doi: 10.1088/0960-1317/18/4/045005. URL https://doi.org/10.1088/0960-1317/18/4/045005.

G. Chen, Y. Gou, and A. Zhang. Synthesis of Compliant Multistable Mechanisms Through Use of a Single Bistable Mechanism. *Journal of Mechanical Design*, 133(8):081007, 08 2011. ISSN 1050-0472. doi: 10.1115/1.4004543. URL https://doi.org/10.1115/1.4004543.

J.-S. Chen and H.-W. Tsao. Static snapping load of a hinged extensible elastica. *Applied Mathematical Modelling*, 37(18):8401–8408, 2013. ISSN 0307-904X. doi: https://doi.org/10.1016/j.apm.2013.03.040. URL https://www.sciencedirect.com/science/article/pii/S0307904X1300214X.

J.-S. Chen and H.-W. Tsao. Dynamic snapping of a hinged extensible elastica under a step load. *International Journal of Non-Linear Mechanics*, 59:9–15, 2014. ISSN 0020-7462. doi: https://doi.org/10.1016/j.ijnonlinmec.2013.10.009. URL https://www.sciencedirect.com/science/article/pii/S0020746213001960.

X. Chen and S. Meguid. Snap-through buckling of initially curved microbeam subject to an electrostatic force. *Proceedings of the Royal Society A: Mathematical, Physical and Engineering Sciences*, 471:20150072–20150072, 04 2015. doi: 10.1098/rspa.2015.0072.

V. Chouvardas, A. Miliou, and M. Hatalis. Tactile displays: Overview and recent advances. *Displays*, 29(3):185–194, 2008. ISSN 0141-9382. doi: https://doi.org/10.1016/j.displa.2007.07.003. URL https://www.sciencedirect.com/science/article/pii/S0141938207000613.

K. A. Cook-Chennault, N. Thambi, and A. M. Sastry. Powering mems portable devices - a review of non-regenerative and regenerative power supply systems with special emphasis on piezoelectric energy harvesting systems. *Smart Materials and Structures*, 17(4):043001, jun 2008. doi: 10.1088/0964-1726/17/4/043001. URL https://dx.doi.org/10.1088/0964-1726/17/4/043001.

F. Cottone, H. Vocca, and L. Gammaitoni. Nonlinear energy harvesting. *Phys. Rev. Lett.*, 102:080601, Feb 2009. doi: 10.1103/PhysRevLett.102.080601. URL https://link.aps.org/doi/10.1103/PhysRevLett.102.080601.

C. L. Dym. *Stability theory and its applications to structural mechanics*. Dover books on engineering. Dover Publications, Mineola (N.Y.), 2002. ISBN 048642541X; 9780486425412.

S. A. Emam and D. J. Inman. A Review on Bistable Composite Laminates for Morphing and Energy Harvesting. *Applied Mechanics Reviews*, 67(6):060803, 12 2015. ISSN 0003-6900. doi: 10.1115/1.4032037. URL https://doi.org/10.1115/1.4032037.

G.-H. Feng and S.-Y. Hou. Investigation of tactile bump array actuated with ionic polymerâmetal composite cantilever beams for refreshable braille display application. *Sensors and Actuators A: Physical*, 275:137–147, 2018. ISSN 0924-4247. doi: https://doi.org/10.1016/j.sna.2018.04.007. URL https://www.sciencedirect.com/science/article/pii/S0924424718301456.

A. Fernandes and J. Pouget. Enhanced Piezoelectric Multilayered Beam: Modelling, Experimental Validation and Application to Actuation. volume ASME 2010 Conference on Smart Materials, Adaptive Structures and Intelligent Systems, Volume 1 of *Smart Materials, Adaptive Structures and Intelligent Systems*, pages 275–284, 09 2010. doi: 10.1115/SMASIS2010-3813. URL https://doi.org/10.1115/SMASIS2010-3813.

A. Fernandes, C. Maurini, and S. Vidoli. Multiparameter actuation for shape control of bistable composite plates. *International Journal of Solids and Structures*, 47(10):1449–1458, 2010. ISSN 0020-7683. doi: https://doi.org/10.1016/j.ijsolstr.2010.02.007. URL https://www.sciencedirect.com/science/article/pii/S0020768310000491.

S. Fu, G. Ding, H. Wang, Z. Yang, and J. Feng. Design and fabrication of a magnetic bi-stable electromagnetic mems relay. *Microelectronics Journal*, 38(4):556–563, 2007. ISSN 0026-2692. doi: https://doi.org/10.1016/j.mejo.2007.03.015. URL https://www.sciencedirect.com/science/article/pii/S0026269207000547. Special Issue of the 6th International Symposium on Quality Electronic Design (ISQED) March 21-23 San Jose, CA.

V. G. A. Goss. The History of the Planar Elastica: Insights into Mechanics and Scientific Method. *Science & Education*, 18(8):1057–1082, Aug. 2009. doi: 10.1007/s11191-008-9166-2.

T. Ikeda. *Fundamentals of Piezoelectricity*. Oxford science publications. Oxford University Press, 1990.

S. Krylov and N. Dick. Dynamic stability of electrostatically actuated initially curved shallow micro beams. *Continuum Mechanics and Thermodynamics*, 22(6):445–468, Sep 2010. ISSN 1432-0959. doi: 10.1007/s00161-010-0149-6. URL https://doi.org/10.1007/s00161-010-0149-6.

S. Krylov, B. R. Ilic, and S. Lulinsky. Bistability of curved microbeams actuated by fringing electrostatic fields. *Nonlinear Dynamics*, 66(3):403, Apr 2011. ISSN 1573-269X. doi: 10.1007/s11071-011-0038-y. URL https://doi.org/10.1007/s11071-011-0038-y.

A. Magnusson, M. Ristinmaa, and C. Ljung. Behaviour of the extensible elastica solution. *International Journal of Solids and Structures*, 38(46):8441–8457, 2001. ISSN 0020-7683. doi: https://doi.org/10.1016/S0020-7683(01)00089-0. URL https://www.sciencedirect.com/science/article/pii/S0020768301000890.

C. Maurini, J. Pouget, and F. dell'Isola. On a model of layered piezoelectric beams including transverse stress effect. *International Journal of Solids and Structures*, 41(16):4473–4502, 2004. ISSN 0020-7683. doi: https://doi.org/10.1016/j.ijsolstr.2004.03.002. URL https://www.sciencedirect.com/science/article/pii/S0020768304001350.

C. Maurini, J. Pouget, and S. Vidoli. Distributed piezoelectric actuation of a bistable buckled beam. *European Journal of Mechanics - A/Solids*, 26(5):837–853, 2007. ISSN 0997-7538. doi: https://doi.org/10.1016/j.euromechsol.2007.02.001. URL https://www.sciencedirect.com/science/article/pii/S0997753807000228.

H. M. Ouakad. Static response and natural frequencies of microbeams actuated by out-of-plane electrostatic fringing-fields. *International Journal of Non-Linear Mechanics*, 63:39–48, 2014. ISSN 0020-7462. doi: https://doi.org/10.1016/j.ijnonlinmec.2014.03.007. URL https://www.sciencedirect.com/science/article/pii/S0020746214000596.

I. Z. Pane and T. Asano. Investigation on bistability and fabrication of bistable prestressed curved beam. *Japanese Journal of Applied Physics*, 47(6):5291–5296, jun 2008. doi: 10.1143/jjap.47.5291. URL https://doi.org/10.1143/jjap.47.5291.

S. Park and D. Hah. Pre-shaped buckled-beam actuators: Theory and experiments. *Sensors and Actuators A: Physical*, 148(1):186–192, 2008. ISSN 0924-4247. doi: https://doi.org/10.1016/j.sna.2008.07.009. URL https://www.sciencedirect.com/science/article/pii/S0924424708004056.

P. Patricio, M. Adda-Bedia, and M. B. Amar. An elastica problem: instabilities of an elastic arch. *Physica D: Nonlinear Phenomena*, 124(1):285–295, 1998. ISSN 0167-2789. doi: https://doi.org/10.1016/S0167-2789(98)00203-6. URL https://www.sciencedirect.com/science/article/pii/S0167278998002036.

A. H. Ramini, Q. M. Hennawi, and M. I. Younis. Theoretical and experimental investigation of the nonlinear behavior of an electrostatically actuated in-plane mems arch. *Journal of Microelectromechanical Systems*, 25(3):570–578, 2016. doi: 10.1109/JMEMS.2016.2554659.

D. Roodenburg, J. W. Spronck, H. S. J. van der Zant, and W. J. Venstra. Buckling beam micromechanical memory with on-chip readout. *Applied Physics Letters*, 94(18):183501, 05 2009. ISSN 0003-6951. doi: 10.1063/1.3129195. URL https://doi.org/10.1063/1.3129195.

J. Schoeftner, G. Buchberger, A. Brandl, and H. Irschik. Theoretical prediction and experimental verification of shape control of beams with piezoelectric patches and resistive circuits. *Composite Structures*, 133:746–755, 2015. ISSN 0263-8223. doi: https://doi.org/10.1016/j.compstruct.2015.07.026. URL https://www.sciencedirect.com/science/article/pii/S026382231500570X.

M. R. Schultz and M. W. Hyer. Snap-through of unsymmetric cross-ply laminates using piezoceramic actuators. *Journal of Intelligent Material Systems and Structures*, 14(12):795–814, 2003. doi: 10.1177/104538903039261. URL https://doi.org/10.1177/104538903039261.

J. Thompson and G. Hunt. *A General Theory of Elastic Stability*. Wiley-interscience publication. J. Wiley, 1973. ISBN 9780471859918.

S. Timoshenko and J. M. Gere. *Theory of elastic stability*. McGraw-Hill, 2nd edition, 1963.

R. Vitushinsky, S. Schmitz, and A. Ludwig. Bistable thin-film shape memory actuators for applications in tactile displays. *Journal of Microelectromechanical Systems*, 18(1):186–194, 2009. doi: 10.1109/JMEMS.2008.2009816.

Z. Wu, R. L. Harne, and K. W. Wang. Excitation-Induced Stability in a Bistable Duffing Oscillator: Analysis and Experiments. *Journal of Computational and Nonlinear Dynamics*, 10(1), 10 2014. ISSN 1555-1415. doi: 10.1115/1.4026974. URL https://doi.org/10.1115/1.4026974. 011016.

H. Xiu and R. B. Davis. Stabilizing higher-order equilibria of post-buckled beams using piezoelectric actuation. *European Journal of Mechanics - A/Solids*, 88:104264, 2021. ISSN 0997-7538. doi: https://doi.org/10.1016/j.euromechsol.2021.104264. URL https://www.sciencedirect.com/science/article/pii/S0997753821000504.

M. I. Younis, H. M. Ouakad, F. M. Alsaleem, R. Miles, and W. Cui. Nonlinear dynamics of mems arches under harmonic electrostatic actuation. *Journal of Microelectromechanical Systems*, 19 (3):647–656, 2010. doi: 10.1109/JMEMS.2010.2046624.

S. Zaidi, F. Lamarque, C. Prelle, O. Carton, and A. Zeinert. Contactless and selective energy transfer to a bistable micro-actuator using laser heated shape memory alloy. *Smart Materials and Structures*, 21(11):115027, oct 2012. doi: 10.1088/0964-1726/21/11/115027. URL https://doi.org/10.1088/0964-1726/21/11/115027.

Z. Zhang, Y. Li, X. Yu, X. Li, H. Wu, H. Wu, S. Jiang, and G. Chai. Bistable morphing composite structures: A review. *Thin-Walled Structures*, 142:74–97, 2019. ISSN 0263-8231. doi: https://doi.org/10.1016/j.tws.2019.04.040. URL https://www.sciencedirect.com/science/article/pii/S0263823119300928.